LANGMUIR

pubs.acs.org/Langmuir
Article

Directing Cell Phenotype: Quantitative Single-Cell Migration Assay Leveraging Tunable Extracellular Surfaces

Logan I. Kaler, Michael C. Robitaille, Joseph A. Christodoulides, Patrick J. Calhoun, Jeff M. Byers, and Marc P. Raphael*

Cite This: *Langmuir* 2025, 41, 13763−13773
Read Online
ACCESS | Metrics & More | Article Recommendations | Supporting Information

ABSTRACT: From *in vitro* cancer research to immunology, single-cell migration assays are among the most common assays for gaining phenotypic insight into the dynamics of adhesion and migration. In general, however, the extracellular environments used in these assays are poorly characterized, which can lead to difficulty interpreting the resulting cellular behavior. Here we introduce a single-cell migration assay which incorporates tunable surfaces that are chemically well-characterized by surface ligand activity (surface activity) quantification. We applied this approach to MDA-MB-231 breast carcinoma cells, measuring single cell morphology, speed, and directionality as a function of cRGD surface activity, controlled via cRGD ligand spacing. Using this approach, we show cell behavior via morphology, migration, and presence of focal adhesions can be directed from amoeboid to mesenchymal-like phenotypes, highlighting tunable surface activity as a reproducible way to direct phenotype.

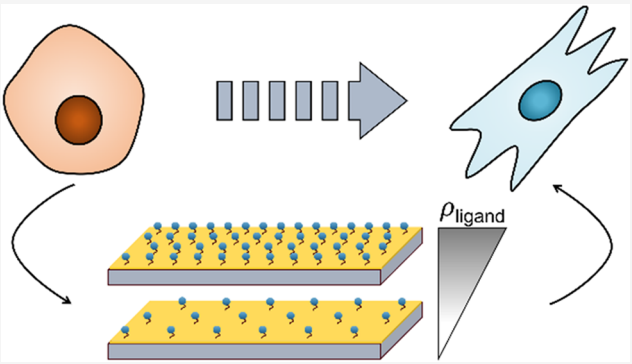

INTRODUCTION

Image-based analysis is increasingly used to characterize cell phenotype, with broad applications in cancer metastasis,[1] cell-based therapies,[2] immune surveillance,[3] and drug discovery.[4] While typically focusing on static snapshots of fixed cells,[5] there is a growing appreciation in the value of time-lapse data, as the information captured by dynamic cellular behavior potentially offers more powerful and biologically relevant cell state classification.[6−8] Single-cell migration assays examine cell movement independent of cell−cell interactions, offering a powerful approach for phenotypic analysis and highlight cell heterogeneity.[9,10]

Cell behavior, and thus phenotype, are known to be extremely sensitive to the chemical and physical properties of the *in vitro* microenvironment.[11−14] Although mesenchymal-like cells are often observed to exhibit a biphasic relationship of their migration speed with adhesion ligand density in two-dimensional (2D),[15,16] this often cited phenomena is greatly affected by the type of ligand, surface immobilization technique, and other environmental factors (e.g., soluble factors).[17−19] Furthermore, cellular sensitivity extends to environmental properties such as substrate stiffness, local ligand density gradients, surface topography, and ligand tether length.[20−23] The ability to tune the properties of the microenvironment is extremely appealing for image-based phenotyping, as it can potentially increase the discriminatory power of assays and screens by directing the desired cells into relevant phenotypes (e.g., a migratory phenotype for drug screens targeting cancer metastasis).

Thus, it is crucial that all single-cell migration assays are conducted in a well-characterized environment with quantifiable chemical and physical inputs. Quantifying these cellular inputs is important for two reasons: reproducibility and quantitative control. Reproducibility—both within a given lab environment and across laboratories, is crucial as seemingly minor changes in experimental conditions can result in significantly different cellular response. For instance, it has been shown that *in vitro* cell media constituents can nonspecifically bind to assay surfaces, reducing surface ligand activity (surface activity) toward their cognate receptor by an order of magnitude or more,[24,25] thereby hindering replication efforts or confounding data interpretation.[26] Similarly, quantitative control over surface inputs allows for varieties of cell phenotypes to be explored, as tuned surface chemistries can give rise to a range of adherent and migratory cell phenotypes.[27]

Received: December 17, 2024
Revised: May 8, 2025
Accepted: May 9, 2025
Published: May 30, 2025

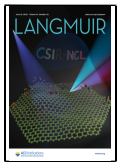

https://doi.org/10.1021/acs.langmuir.4c05135
Langmuir 2025, 41, 13763−13773

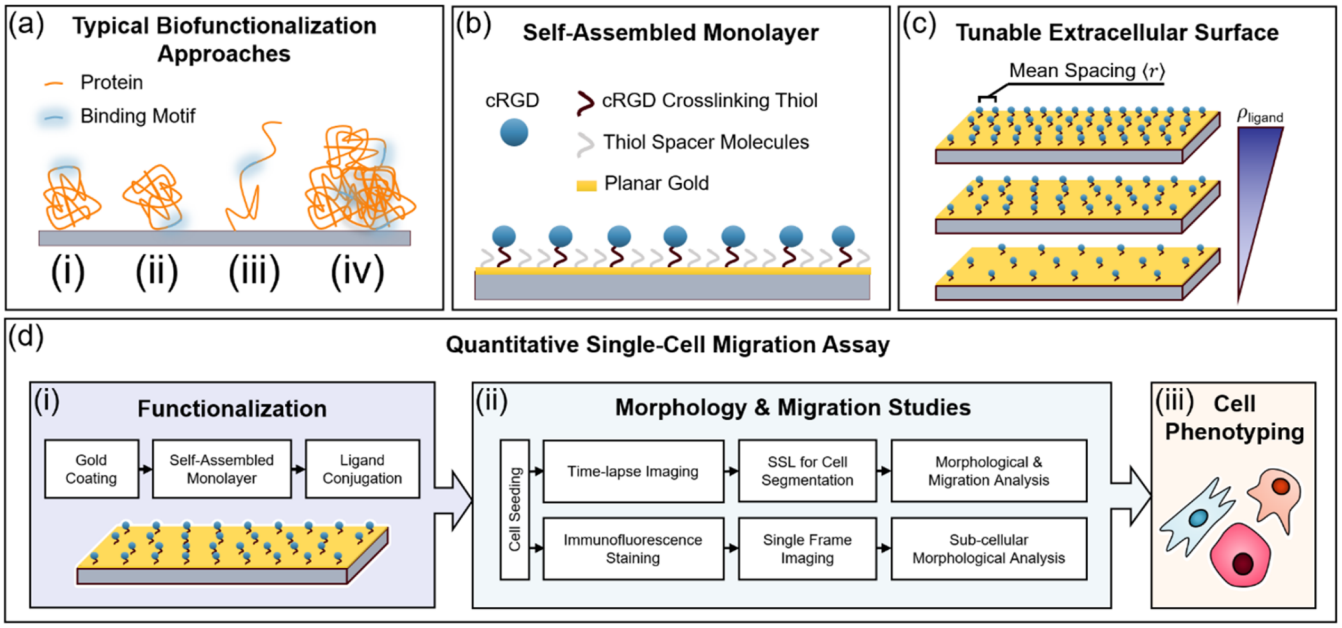

Figure 1. 2D migration assay surface biofunctionalization approaches and workflow for single-cell migration assay. (a) Protein functionalized surfaces (e.g., fibronectin) in which the binding motif (e.g., RGD) is represented in blue. The proteins can be (i) advantageously orientated for engaging membrane bound receptors, (ii) disadvantageously orientated for engaging membrane bound receptors, or alternatively, binding can be blocked by nonspecifically bound media components, (iii) denatured, which alters the stiffness and tether length and (iv) clumped, which alters topography and stiffness. (b) Alkanethiol based self-assembled monolayer formed atop a glass/Au substrate with the cell adhesion peptide (*e.g.* cRGD) represented by a blue dot. (c) By design, the peptides are accessible, tunable in their mean spacing ($\langle r \rangle$), have a prescribed tether length, and uniform topography and stiffness. (d) Workflow for single-cell migration assay utilizing quantified surfaces to distinguish cell phenotypes: (i) Gold surfaces are functionalized by coating with self-assembled monolayer and subsequent conjugation with cRGD ligand. (ii) For morphology and migration studies, cells are seeded on the functionalized surface and undergo two separate pipelines: (1) monitored time-lapse imaging and self-supervised machine learning (SSL) cell segmentation for morphological and migration analysis and (2) immunofluorescent staining followed by single frame imaging for subcellular morphological analysis. (iii) The resulting data is combined to determine cell phenotype.

Given the importance of quantifying these biofunctionalized surfaces, the scarcity of chemical surface characterization in literature reports and for commercially available products is problematic. The typical commercial product data sheet will report the molecule used to coat the surface (e.g., fibronectin, collagen) and the cell type used to test the biofunctionalized surface for migration and viability. In the peer-reviewed literature it is more typical to report the solution concentration of the surface-coating molecule and its incubation time with the surface. None of this information is sufficient to answer the key questions now known to influence cell phenotype as illustrated in Figure 1a: (i) Surface activity: What fraction of the surface bound molecules can actively bind cell receptors? (ii) Bioavailability: Is the surface activity being negatively impacted by improper orientation or interactions with other media constituents? (iii) Stiffness and linker length: If the ligands are proteins, are they denatured? (iv) Stiffness and topography: Are the molecules present as a monolayer or in multilayers, or clumps? For example, fibronectin (Fn) coatings are one of the most common biofunctionalized surfaces utilized in cell biology via adsorption to the underlying substrate. However, Fn adsorption characterization via Quartz Crystal Microbalance with Dissipation (QCM-D) reveals that commonly used soluble concentrations can result in significantly different film thickness (Figure S1), highlighting the entanglement of multiple physical inputs associated with altering ligand surface density in this widely used method. This example raises questions about confounding physical and chemical inputs to cellular response through poorly characterized biointerfaces, and highlights the need for quantitative surface characterization for single-cell migration assays to achieve their potential of being both reproducible and more generally predictive.

Alkanethiol based self-assembled monolayers (SAMs) have long been known as idealized biointerfaces,[28] but only recently have quantified surface activities been linked to *in vitro* assay outcomes.[29] Here we provide a platform for developing highly quantified, reproducible migration assays which addresses these questions and demonstrate the range of migratory plasticity that can be uncovered by systematically tuning biochemical surface activity through the use of SAMs (Figure 1b) and subsequent adjustment of the mean spacing between cyclic RGD peptide (cRGD) peptides (Figure 1c). Importantly, the thiol design specifications define the stiffness, linker length, and bioavailability due to direct conjugation of cRGD to the surface,[29] while the ratio of thiol spacer molecules to cRGD cross-linking thiol varies the surface activity by adjusting the mean spacing between cRGD ligands. This platform is incorporated into a workflow for utilizing biofunctionalized surface in morphology and migration studies to enhance cell phenotyping (Figure 1d).

To characterize the surface activity, a concurrent control technique is applied in which surfaces for activity characterization via surface plasmon resonance (SPR) are prepared in parallel with those used for the single-cell migration studies.[29] SPR can also be employed to measure ligand bioavailability in the presence of complex cell media preparations. Surface monolayers and subnanometer roughness are achieved by using thiol-based SAM techniques and verified by atomic force microscopy (AFM).[24]

https://doi.org/10.1021/acs.langmuir.4c05135
Langmuir 2025, 41, 13763−13773

In this study, cRGD was utilized to promote cell adhesion and migration, ensuring that denaturation was not a concern and enabling the linker length to be synthetically controlled via SAM layer design. We applied this approach to single-cell migration assays of MDA-MB-231 breast carcinoma cells and measured cell morphology, speed, and directionality as a function of surface activity. While a host of morphological parameters such as cell area and circularity varied monotonically with cRGD surface activity, the corresponding cell speeds were decidedly nonmonotonic − increasing then decreasing then increasing again as a function of surface activity, independent of the applied migratory model. Immunofluorescence for vinculin and F-actin revealed that focal adhesions and stress fibers were only present in cells on substrates with higher surface activity. These results highlight that well-tuned chemical environments can reproducibly elicit several migratory phenotypes that exhibit distinct morphology and migration characteristics ideal for image-based phenotyping assays and emphasize a need for controlled extracellular environments in single-cell assays.

EXPERIMENTAL SECTION

Recombinant human $\alpha_v\beta_3$ integrins (R&D Systems, #3050-AV-050) were reconstituted in 20 mM Tris buffered saline (TBS), pH 7.4, and 0.9% NaCl (Sigma, #T5912). The RGD-based peptide cRGDfK (cRGD, Peptides International, #PCI-3661-PI) was reconstituted in modified Dulbecco's phosphate buffered saline (DPBS, Thermo, #28344) titrated with sodium hydroxide to pH 8.0. The self-assembled monolayer (SAM) thiols, SH-$(CH_2)_{11}$-EG_5−OH (SPO) and SH-$(CH_2)_{11}$-EG_6-COH_2−COOH (SPC) (Prochimia Surfaces Sp., TH 001-m11.n5 and TH 003-m11.n6) were reconstituted in 200 proof, anhydrous ethanol. *N*-hydroxysulfosuccinimide (sulfo-NHS) and 1-ethyl-3-[3-(dimethylamino)propyl]carbodiimide hydrochloride (EDC) from Thermo Scientific were dissolved in 18 MΩ DDW immediately before use. Ethanolamine (Sigma, #E905) was diluted in pH 7.4 DPBS to 0.1M. Ultrapure sodium dodecyl sulfate (SDS) solution (Invitrogen, #15553027) was diluted with 18 MΩ DDW unless otherwise specified.

For SPR measurements, commercially available bare gold sensor chips were purchased from Cytiva (SIA Kit Au). For *in vitro* studies, 20 nm Au thin films were deposited on 25.4 mm diameter, No. 1.5 glass coverslips by e-beam evaporation as previously described. The gold film was thin enough to allow for phase contrast microscopy techniques to be employed but thick enough for a continuous film to be formed on the substrate. The surface roughness, stiffness and tether length are all well-defined by the gold deposition and thiol design specifications as previously described.[29] The cRGD surface activity was systematically varied by adjustments of the SPO/SPC ratio and quantified by SPR as described below.

For immunofluorescent studies, a Temescal e-beam evaporation system FC2000 was used to deposit a 20 nm Au thin film onto the surface of a commercially available 1.5 glass-bottom 24-well plate (MatTek, P24G-1.5−13-F). Care was taken so that the deposition direction was perpendicular to the substrates to minimize side wall deposition. The e-beam source was preconditioned to maintain a stable deposition rate of 2 Å/s and accurate thickness. A masking technique was employed to shield specific areas/wells of the plate, for control measurements. The cRGD surface activity was systematically varied by adjusting the SPO/SPC ratio as described below. For Fn immunofluorescent studies, human plasma Fn (Gibco, #33016105) was diluted down to the desired concentration (1, 5, 10, 25, 50, and 100 μg/mL) and drop coated directly onto MatTek dishes and allowed to adsorb for 1 h at room temperature, followed by 3 rinses with DDW prior to introduction of cells.

Quartz Crystal Microbalance with Dissipation (QCM-D) Characterization of Fn Adsorption. Adsorption measurements were conducted on a Qsense Analyzer (Biolin Scientific) on Qsensor QSX 303 SiO_2 sensors (Biolin Scientific). Each sensor was allowed to equilibrate in their flow cell under running 10 mM PBS buffer until sensor drift was observed to have less than 1 Hz drift/h. Human plasma Fn (Gibco, #33016105) was diluted down to the desired concentration (1, 5, 10, 25, 50, and 100 μg/mL) and was introduced to the sensor at a flow rate of 100 μL/min, and subsequently rinsed with buffer to remove any lightly bound Fn. The subsequent frequency and dissipation shifts were fit using a Voight viscoelastic model to estimate the amount of adsorbed material on the SiO_2 surface and resulting film thickness in the Qtools software (Biolin Scientific). Experiments were conducted in triplicate for each Fn concentration.

Chip Functionalization and Concurrent Surface Plasmon Resonance (SPR) Controls. For SPR studies using the Biacore 8K instrument, SIA bare gold sensor chips were cleaned down to the bare gold surface by a reactive ion etch (RIE) system utilizing 5% hydrogen, 95% argon gas mixture with the pressure regulated at 300 mT and the RF power at 40 W, and then functionalized with a two component SAM consisting of SPO and SPC as previously described.[29] The chips were immersed for 18 h in an 0.5 mM ethanolic-based thiol solution (room temperature) with a SPO to SPC ratios (and estimated ligand−ligand spacing $\langle r \rangle$) of 25:1 (2 nm), 250:1 (6 nm), 2500:1 (19 nm), 25k:1 (59 nm) and 250k:1 (187 nm). The chips were then rinsed with EtOH, dried under flowing nitrogen gas, and mounted atop the Biacore SIA sensor inserts according to the manufacturer's instructions. Estimated ligand−ligand spacings were calculated as previously described.[29]

Activation of the SPC component with cRGD consisted of flowing a 33:133 mM ratio of sulfo-NHS:EDC for 5 min, followed by flowing 0.35 mg/mL cRGDfK for 5 min. Next, unreacted −COOH groups were blocked by flowing 0.1 M ethanolamine for 5 min. Finally, nonspecifically bound reagents were removed by flowing 0.5% SDS (w/v, DDW) for 5 min. For all immobilization steps the flow rate was 10 μL/min and 18 MΩ DDW was used a running buffer. The Biacore 8K design incorporates 8 channels, each consisting of sensing lane paired with a reference lane for the subtraction of nonspecifically bound analyte. The same immobilization protocol was used for both reference and sensing lanes with the exception that no cRGD was applied to the reference lane.

As with the SPR chips, the Au coated coverslips were cleaned down to the bare gold surface using a RIE system with the same gas, pressure and power conditions described above and then functionalized with a two component SAM by immersion for 18 h in an ethanolic-based thiol solution (0.5 mM). For the Au thin film biofunctionalization, the SPR self-assembled monolayer and immobilization procedures were repeated except all solutions were manually drop coated atop the chips and extensively washed with DDW. As a negative control for cell adhesion studies, additional *in vitro* chips were prepared consisting of only SPO thiols. Cells were in serum-free media when introduced to the SAMs to preserve the surface activity of the cRGD.

SPR-Based Kinetic Rate Constants and Surface Activity Measurements. TBS + 0.5 mM $MnCl_2$ was used as the running buffer for all kinetic rate constant and surface activity measurements with recombinant human $\alpha_v\beta_3$ integrins introduced at a flow rate was 30 μL/min for all steps. Before the integrin introduction, the chip sensing surfaces were normalized using a 70% glycerol solution (BiaNorm, Cytiva) and then rinsed with 0.25% SDS (w/v, TBS) and multiple TBS rinses (400 s each). All SPR experiments incorporated at least one control channel (blank) of only running buffer used to subtract out instrumental drift. The plotted SPR response curves have the reference lane and the buffer control channel subtracted.

***In Vitro* Cell Culture.** MDA-MB-231 cells (ATCC, #HTB-26) were cultured in DMEM supplemented with 10% fetal bovine serum (ATCC) and maintained at 37 °C and 5% CO_2. Prior to seeding on functionalized Au films, cells were harvested in their logarithmic growth phase,[29] and trypsinized by adding 1 mL of trypsin-EDTA (ATCC) at 37 °C for 3−4 min before the addition of DMEM (no serum). The cells were spun down at 125*g* for 5 min and the pellet resuspended in 5 mL DMEM (no serum). Cells were spun down

https://doi.org/10.1021/acs.langmuir.4c05135
Langmuir 2025, 41, 13763−13773

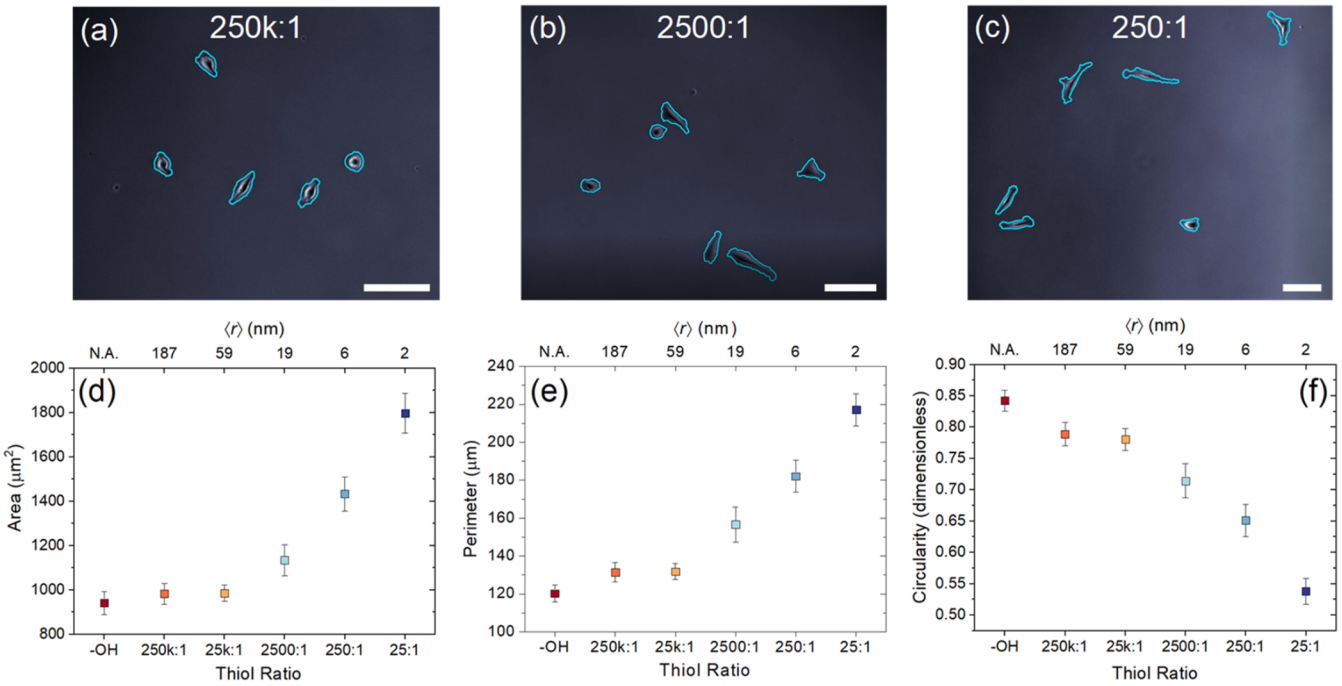

Figure 2. Morphological phenotyping as a function of surface activity. Representative images are shown for three surfaces (a) 250k:1, low cRGD activity, (b) 2500:1, moderate cRGD activity (c) 250:1, high cRGD activity. The automated cell segmentations (blue outlines) from phase contrast images were used to generate mean cell area, perimeter, and circularity data shown in (d–f). Each datum displays the average and standard error of mean from ∼75 segmented cells, pooled from technical and biological replicates and time averaged over the 7-h migration study. The contrast has been enhanced in images (a–c) to highlight cell shape. Scale bar = 100 μm. Mean spacing ($\langle r \rangle$) displayed on top x-axis for (d–f).

again and resuspended in serum-free media to thoroughly eliminate all trypsin and serum components. As an additional negative control for the cell adhesion studies, the cells were resuspended in a DMEM-based solution containing 1 mM of cRGD for 60 min before drop coating on 25:1 thiol ratio chips. Cells exposed to cRGD in solution in this manner remained rounded and did not spread on the chips (data not shown).

Live Cell Microscopy. Live cell imaging was performed using phase contrast illumination with a 10×, 0.9 numerical aperture objective. A heated stage and temperature-controlled enclosure held the stage temperature at 37.0 ± 0.04 °C (Zeiss). Humidity and CO_2 were regulated at 98 and 5%, respectively. Cells were added to the functionalized chip to achieve cell densities of approximately 27 cells/cm^2 (∼8 cells per field of view) with image acquisition typically beginning within 20 min. Time-lapse, live-cell microscopy was performed every 10 min utilizing an automated X, Y stage to image 10–20 fields of view (FOV) per time point. Live cell imaging experiments were performed for at least 15 h.

Cell Morphology and Migration Analysis. To ensure objective live cell segmentation and analysis from the imagery, a completely automated self-supervised machine learning (SSL) algorithm was employed that required no curated training data or parameter tuning.[30] For each image, the algorithm outputs metadata which includes the outlines of the segmented cells, their centroid positions, as well as morphological parameters such as cell area, Feret min/max, and circularity.

For each thiol surface ratio at least 75 individual cells were selected from 3 biological replicates (BRs) with roughly 25 cells per BR. BRs were conducted on different days with newly prepared cRGD surfaces using different cell passages. Cells were given at least 7 h to reach homeostasis with the surface based on morphological profiling,[29] after which they were manually selected from the metadata using the following set of rules: each cell was tracked for 7 h during which the cell did not contact other cells and the cell did not enter mitosis.

In addition to analyzing the extracted morphological parameters, cell migration was assessed using several models. The first model considered is instantaneous velocity, calculated as $\Delta r_i/\Delta t$, where Δr_i represents the distance traversed by the cell's centroid during the i-th wait time point, and Δt is the wait time between images (10 min). Another model used is the end-point directionality index, which is the ratio of the cell's centroid distance from the origin at the end of the observation period (7 h), denoted as d_{end}, to the total distance traversed, represented as $d_{end}/\sum_i \Delta r_i$. The mean square displacement (MSD) time exponent was also evaluated, with the relationship given by MSD $\propto t^{\alpha}$, where $\alpha = 1$ indicates purely diffusive migration, $\alpha > 1$ denotes 'superdiffusive' migration, and $\alpha < 1$ is considered 'subdiffusive'. Lastly, the persistent random walk (PRW) speed was analyzed according to the methodology outlined by Wu et al.[31]

Immunofluorescence Staining and Analysis. MDA-MB-231 cells were cultured in serum-free DMEM on functionalized Au films for 8 h before fixation. The −OH condition served as a mock and was treated with cRGD in the absence of the SAM. Cells were quickly rinsed three times with ice cold phosphate-buffered saline with Ca^{2+} and Mg^{2+} (PBS++; Gibco, 14190–144) before treatment with 4% paraformaldehyde (Thermo Scientific, 28908) in PBS++ for 20 min at room temperature. Cells were then rinsed with PBS++ before immunofluorescence staining.

Fixed MDA-MB-231 cells were rinsed three times with room temperature PBS++ before treatment with 0.5% Triton X (Millipore Sigma, X100–100 ML) for 10 min. After rinsing three times with room temperature PBS++, cells were treated with blocking buffer containing 5% goat serum (Invitrogen, 31873) in PBS++ for 1 h at room temperature. Blocking buffer was then replaced with mouse antivinculin (Invitrogen, V9131) primary antibody at 1:500 dilution in PBS++ with 1% Bovine serum albumin (BSA; Sigma, A9647–100G) for 1 h at room temperature. Cells were rinsed with PBS++ with 0.05% Tween-20 (Sigma, P2287) in 5- and 10 min intervals before treatment with 1:500 dilution Alexa Fluor 488 goat antimouse IgG (Jackson ImmunoResearch Laboratories, 115–545–003), 1:500 dilution Alexa Fluor 555 phalloidin (Invitrogen, 30106), and DAPI NucBlue Fixed Cell Stain ReadyProbes (Invitrogen, R37606) for 1 h at room temperature. Following staining, cells were rinsed with PBS++ with 0.05% Tween-20 in 5- and 10 min intervals, covered with parafilm and aluminum foil, and stored at 4 °C until imaged.

https://doi.org/10.1021/acs.langmuir.4c05135
Langmuir 2025, 41, 13763–13773

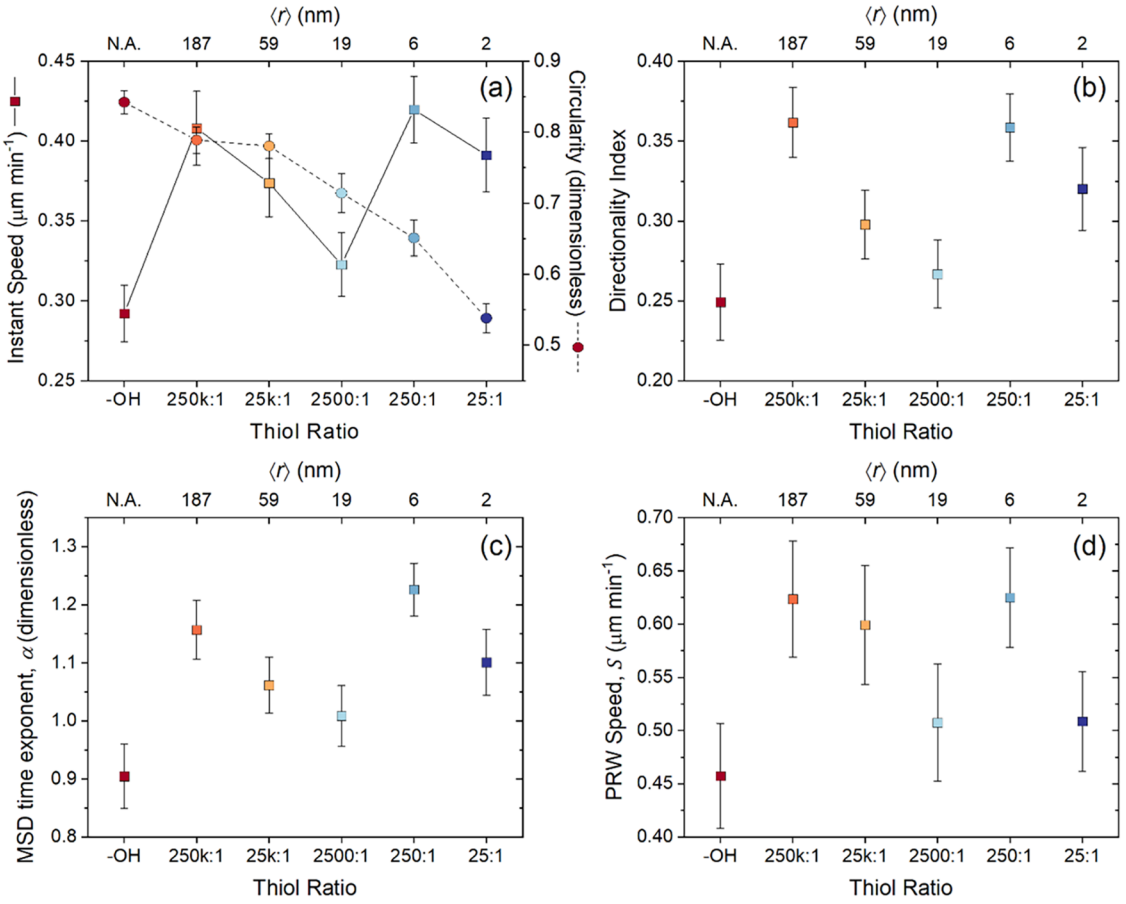

Figure 3. Cell speed and directionality parameters as a function of surface activity. (a) Cell circularity from Figure 2f (circles, dashed line) coplotted with the cell instantaneous speed (squares, solid line). (b) Directionality index. (c) Mean square displacement (MSD) time exponent, α. (d) Persistent random walk (PRW) speed, S. Each datum displays the average and standard error of the mean from ∼75 segmented cells, pooled from technical and biological replicates and time averaged or fit over the 7-h migration study. Mean spacing ($\langle r \rangle$) displayed on top x-axis for (a−d).

Immunofluorescent cells were imaged using oil-immersion 60× objective on Nikon A1 confocal equipped with 405, 488, 561, and 640 nm laser lines. The resulting images were analyzed for focal adhesions and F-actin using CellProfiler.[32] Objects identified from the vinculin immunofluorescence are referred to as focal adhesions, whereas objects identified from the phalloidin immunofluorescence are referred to as F-actin. For each image, morphological parameters of the immunofluorescent objects (i.e., focal adhesions or F-actin) were calculated, including the area and max Feret diameter (referred to as length, l). Statistical analyses and graphical representations of these data were prepared using Origin Pro (OriginLab Corporation; Northampton, MA).

RESULTS AND DISCUSSION

This work utilized biofunctionalized surfaces in morphology and migration studies to enhance cell phenotyping. The cRGD surface activity was systematically tuned by varying the ratio of thiol spacer molecules (SPO) to those with functional groups for cross-linking to cRGD (SPC). These surfaces ranged from all SPO surfaces (−OH) to a 25:1 SPO/SPC ratio and surface activity quantified by SPR using recombinant human $\alpha_v\beta_3$ integrins as a probe (Figure S2).

MDA-MB-231 breast cancer cells were seeded without serum on the functionalized surfaces and analyzed for morphology (Figure 2) and migration (Figures 3 and 4) over a 7-h period. Cell morphological phenotype varied monotonically from more circular (Figure 2a) to elongated (Figure 2b,c) with increasing surface activity. SSL for cell segmentation was employed to automatically extract morphological features including mean cell area, perimeter, and circularity (Figure 2d−f). The cell spread area and perimeter increased with cRGD surface activity and circularity decreased, consistent with the observation of the cells increasing in elongation with increasing surface activity.

In contrast, Figures 3 and 4 highlight the more complex relationship between cell shape and migratory speed. The cells achieved their highest speeds on both low activity surfaces (250k:1) and high activity surfaces (250:1), while exhibiting largely circular and significantly more elongated morphologies, respectively (Figure 3a). To ensure these results were not model dependent we analyzed cell speed and directionality using a range of models including directionality index (Figure 3b), mean square displacement (MSD) time exponent (Figure 3c) and persistent random walk (PRW) speed (Figure 3d). In all cases the pattern of increasing and decreasing migration speed and directionality index with surface activity were consistent.

Representative migration trajectories as well as the corresponding cell outlines are depicted in Figure 4a, showing that cells on OH and 2500:1 surfaces typically traveled shorter distances and have stable morphologies during the observed migration period. The subtle changes in cell motility via tuning surface activity are shown in Figure 4b by the log−log plots of the MSD versus time, showing that both 250k:1 and 250:1 elicit slightly superdiffusive motion with $\alpha \approx 1.2$, and

https://doi.org/10.1021/acs.langmuir.4c05135
Langmuir 2025, 41, 13763−13773

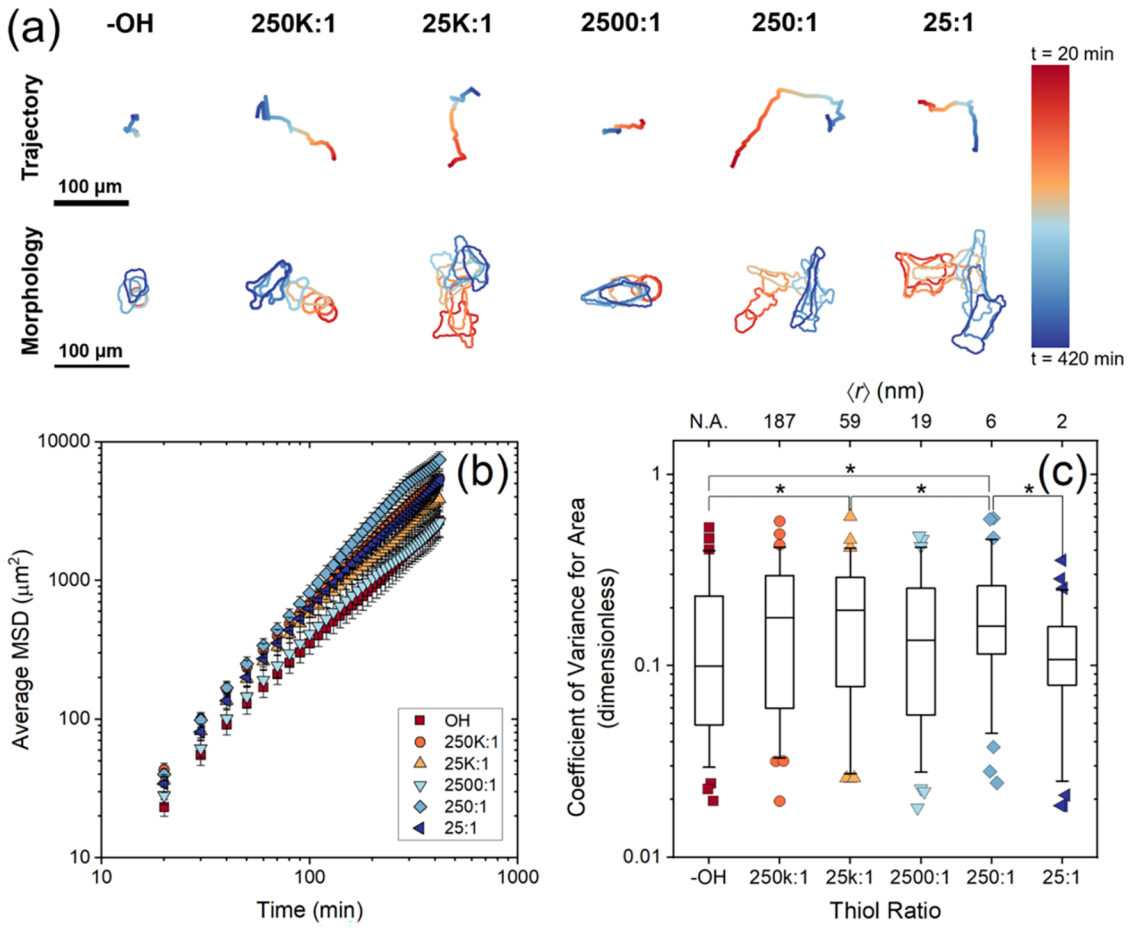

Figure 4. Cell dynamic morphology as a function of surface activity. (a) Representative cell trajectories and morphologies for each surface activity. Traces show cell trajectory and morphology over 7 h with color scale indicating time. Scale bar represents 100 μm. (b) Average mean square displacement (MSD) for all cells. Error bars indicate standard error of the mean. (c) Coefficient of variance for the spread area measured for each individual cell to characterize fluctuations in morphology. Whiskers are drawn down to the 5th percentile, up to the 95th percentile, and outliers are plotted as points. Data set statistically analyzed with Kruskal–Wallis test and Dunn's test for multiple comparisons: $*p < 0.05$. Mean spacing ($\langle r \rangle$) displayed on top x-axis for (c).

subdiffusive motion ($\alpha < 1$) is only achieved on the mock (−OH). Furthermore, slower cell migration is associated with lower fluctuations in cell spread area (Figure 4c), which is consistent with less observed lamellipodia protrusions/retractions observed on the OH and 2500:1 surfaces. These fluctuations in cell spread area due to lamellipodia protrusions/retractions were quantified by measuring the coefficient of variation for the area of individual cells. A higher coefficient of variation indicated more changes in cell area over time, whereas a lower coefficient of variation indicated fewer changes in cell area over time. The combined data give a clear example of how quantitatively tuning the extracellular environment can expose cellular migratory plasticity.

The architectural differences in the cell cytoskeleton elicited by tuning the cRGD surface activity were highlighted by immunofluorescent staining of fixed MDA-MB-231 cells (Figure 5). Based on the observed differences in migration and morphology, the −OH, 250k:1, 2500:1, and 250:1 thiol ratios were chosen for immunofluorescence staining. While there were differences observed at the 25k:1 and 25:1 ratios, the selected ratios were representative of the extremes: −OH had high circularity and low speed, 250k:1 had high circularity and high speed, 2500:1 had lower circularity and lower speed, and 250:1 had lower circularity and high speed. In the mock (−OH) and lower surface activity (250k:1 and 2500:1) conditions (Figure 5a–c), the F-actin was predominately diffuse and cortical in arrangement, with typical stress fibers present only at the higher surface activity (250:1), characterized by their anchoring at large focal adhesions (Figure 5d). Few focal adhesions were observed in the mock, with small focal adhesions ($l < 1$ μm) observed in the lower surface activity conditions (250k:1 and 2500:1). Focal adhesion and F-actin morphology analysis showed increased area in response to increased surface activity (Figure 5e), which corresponded with an increase in length (Figure 5f). The mature focal adhesions were calculated based on the length, with significant increase in the number of mature focal adhesions on the 250:1 surface condition (Figure 5g). To compare how the quantified cRGD surfaces influence cell phenotype to more common Fn-coated surfaces, we conducted immunofluorescence experiments on 0 (mock), 5, 10, 25, 50, and 100 μg/mL surfaces (correlated with QCM-D measurements), with representative images shown in Figure S3a. Cells seeded on lower Fn density (0, 5, and 10 μg/mL) exhibited a round morphology with F-actin observed as diffuse in nature and cortical in arrangement, and vinculin similarly diffuse − no stress fibers or visible mature focal adhesions were observed under these conditions. Cells seeded on higher Fn density (25, 50, and 100 μg/mL)

https://doi.org/10.1021/acs.langmuir.4c05135
Langmuir 2025, 41, 13763−13773

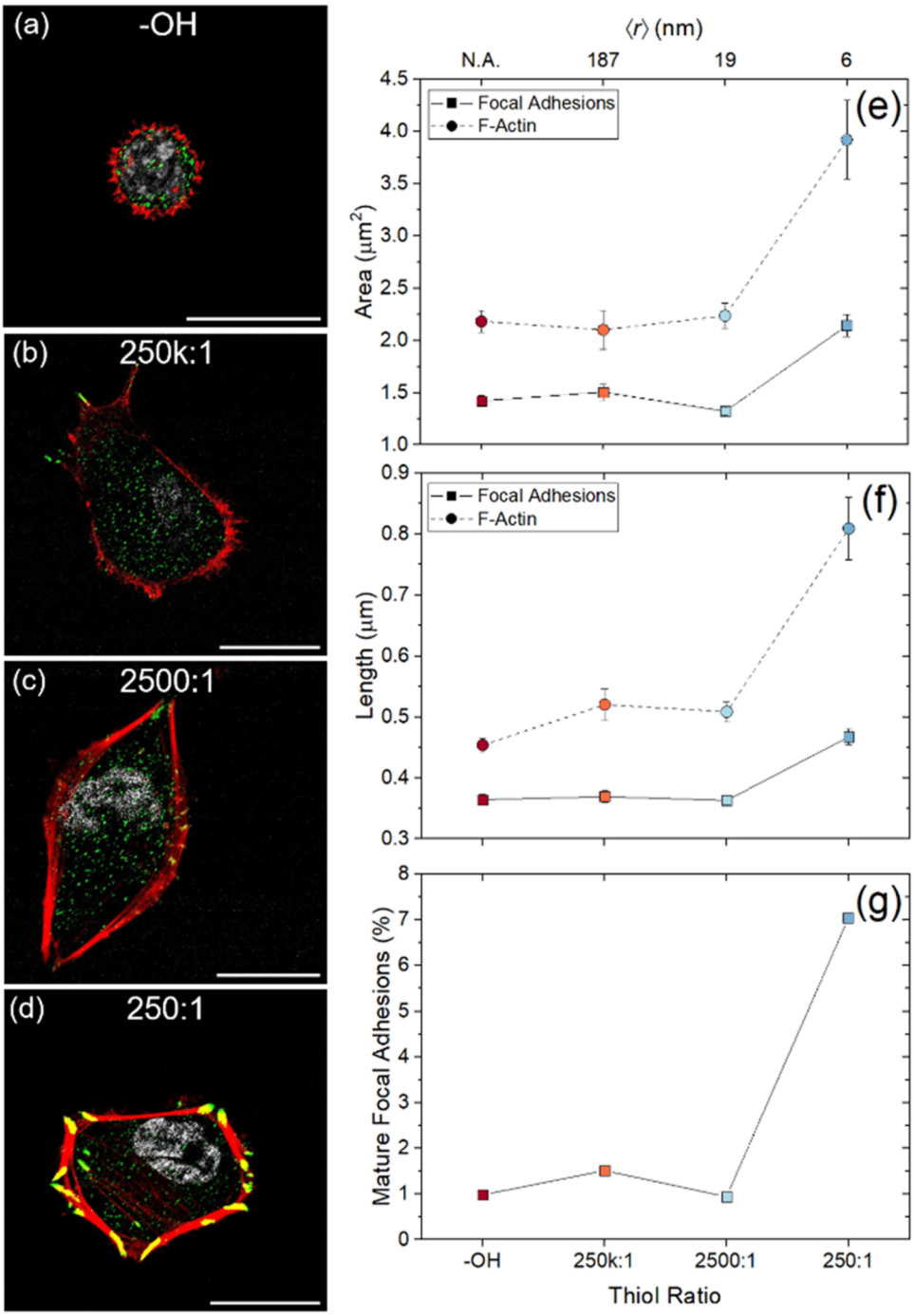

Figure 5. Immunofluorescent staining for focal adhesions and F-actin in response to varying surface activity. (a–d) Representative images for each condition are shown with vinculin (green) staining for focal adhesions, phalloidin (red) staining for F-actin, and DAPI for DNA (gray). Colocalization of vinculin and phalloidin appears yellow. (e, f) Cell Profiler analysis was used to calculate (e) area and (f) length of focal adhesions (black squares, solid line) and F-actin (blue circles, dashed line). (g) Percentage of focal adhesions with a length >1 μm; considered mature focal adhesions. Each datum indicates the mean and standard error of the mean pooled from 6 technical and biological replicates with ∼25 cells per replicate. Scale bar = 20 μm. Mean spacing ($\langle r \rangle$) displayed on top x-axis for (e–g).

cells exhibited an elongated and spread-out morphology with F-actin readily observed in stress fiber architectures that anchor at abundant and clearly visible mature focal adhesions under these conditions. Focal adhesion and F-actin morphology analysis showed a significantly increased area on higher Fn density surfaces (25, 50, and 100 μg/mL) compared to lower Fn density surfaces (0, 5, and 10 μg/mL, Figure S3b).

Fabricated or engineered microenvironments are a fundamental research platform for cell biology and foundational to image-based cell analysis. However, most techniques infer or assume ligand surface activity in lieu of quantitative measurements. In this work, we have expanded on a dual SPR/*in vitro* assay with well-characterized surface activity[24,29] to tune the extracellular environment to quantify single-cell migratory phenotypes. Through precise and reproducible modulation of

https://doi.org/10.1021/acs.langmuir.4c05135
Langmuir 2025, 41, 13763–13773

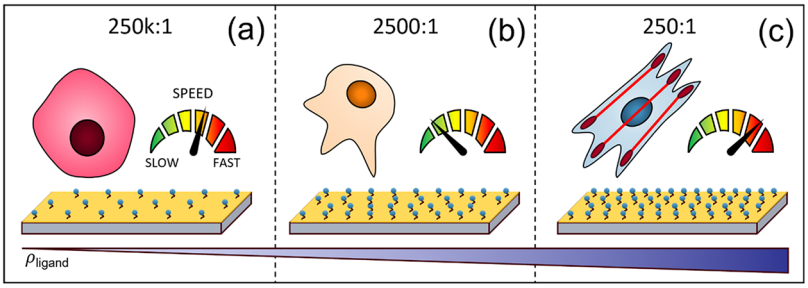

Figure 6. Single-cell migration assay modulates MDA-MB-231 cell phenotype. (a–c) Cell morphology, migratory speed, and cytoskeletal architecture varies with increasing surface activity (represented by blue dots). Mature focal adhesions are shown as dark red ovals and elongated F-actin filaments are shown as red lines.

cRGD spacing, MDA-MB-231 breast cancer cells increased in spread area and elongation with increased cRGD surface activity (Figure 2). However, cell speed, migration directionality, and fluctuations in spread area were found to rise, fall, and rise again with increased cRGD surface activity (Figures 3 and 4). Immunofluorescence staining indicated larger, mature focal adhesions and large F-actin filaments only present on high activity surfaces (250:1, Figure 5) with an average ligand-spacing of $\langle r \rangle \approx 6$ nm. Interestingly, despite a relatively low ligand-spacing of $\langle r \rangle \approx 19$ nm on 2500:1 surfaces, our results indicate that this is not enough available cRGD to sustain efficient/fast focal-adhesion based mesenchymal migration under these conditions. In contrast, mature focal adhesions and large F-actin filaments were observed in cells seeded on Fn concentrations ≥25 μg/mL (Figure S3), which coincides with adsorbed films that exceed a monolayer of Fn (Figure S1). While it is extremely difficult to estimate the average ligand-spacing of adsorbed Fn layers, these results highlight the issues of interpretability of underlying ECM properties when relating the soluble concentration of adsorbed molecules to cellular response (e.g., changes in surface ligand density versus surface stiffness/topography).

Cancer cells primarily use two different modes to migrate individually: mesenchymal and amoeboid.[9,33−35] Mesenchymal-migrating cells use integrins and associated focal adhesion proteins to adhere tightly to their substrate, resulting in elongated cell morphology. In contrast, cells exhibiting amoeboid migration have low adhesive interactions, resulting in a rounded cell morphology.[34−36] Previous studies have shown that MDA-MB-213 cells can exhibit both mesenchymal and amoeboid motility.[33,37−40] We were able to replicate these behaviors by tuning the extracellular environment, as illustrated in Figure 6. At low ligand density (250k:1), cells were circular, lacked mature focal adhesions and large F-actin stress fibers, and displayed faster migration, typical of an amoeboid phenotype (Figure 6a). Interestingly, the enhanced speed at lower surface activity resulted in more persistent migration (Figure 3b). While amoeboid migration is characterized by frequent changes in direction and fast migration, at longer time scales the migration has been shown to resemble a persistent random walk.[41] Given the longer time scale of the experiments (7 h), persistent random walk movement was observed. At medium ligand density (2500:1), cells showed moderate spreading but still lacked mature focal adhesions and large F-actin filaments, and exhibited slower migration, indicative of a slow-migrating intermediate phenotype where the cells exhibit spreading but lack the robust adhesions and large stress fibers observed in a mesenchymal phenotype. (Figure 6b). At high ligand density (250:1), cells became elongated, developed mature focal adhesions and large F-actin stress fibers, and demonstrated fast migration, characteristic of a fast-migrating mesenchymal phenotype (Figure 6c). Elucidating molecular mechanisms of these phenotypic shifts (e.g., RhoA/RAC signaling) would greatly aid in defining these intermediatary phenotypes, and will be incorporated into future studies utilizing this platform.

These results highlight two important facets of the proposed *in vitro* experimental framework. The first is that morphological profiling alone can miss important phenotypic information. The cell area, elongation, and focal-adhesion and actin organization increase monotonically with surface activity, indicating increased cell spreading and adhesion which is indicative of a mesenchymal phenotype. However, if this data is combined with the cell migration data, it becomes apparent that there is a distinct phenotype between the amoeboid and mesenchymal phenotypes. The migration data points to a third slow-migrating intermediate phenotype that is distinguished by not increasing area and decreasing circularity, but by the decrease in migration speed. This result highlights that dynamic morphology and migration data can reveal the subtle spectrum of environmentally induced phenotypes, offering an appealing avenue for applications ranging from drug discovery to stem-cell differentiation.

The second important aspect is that surface activity, while often overlooked *in vitro*, offers a quantitative and reproducible method to direct cell phenotype with greater fidelity compared to standard migration assays. While single-cell migration studies are commonly used, there is currently no standardization in the field. Studies have shown a biphasic relationship between cell speed and surface ligand concentration;[15,18,42,43] however, the surface activity—as well as other important physical parameters—is not directly measured in those publications but inferred, preventing direct comparison between studies or to the results reported here. For instance, He et al. utilized block copolymer micellar nanolithography for precise positioning of RGD peptides for migration study.[44] However, we have previously shown that even small amounts of serum can significantly reduce surface activity,[24] making a direct comparison between experimental results difficult. Here, our quantitative *in vitro* migration assay reveals a more complex relationship with cell speed regarding surface ligand density, with the quantification of surface activity on alkanethiol SAMs an appealing approach to ensure interlaboratory reproducibility.

While this single-cell migration assay platform addresses the need for a quantifiable and reproducible extracellular environment, we acknowledge the assay was designed using a single type of cRGD (cRGDfK) and a single type of integrin ($\alpha_v\beta_3$)

https://doi.org/10.1021/acs.langmuir.4c05135
Langmuir 2025, 41, 13763−13773

was used for SPR experiments. The cRGD ligand is the most studied of the integrins that can specifically bind $\alpha_v\beta_3$, which is overexpressed in most tumor cells,[45] making it ideal for studying cancer cell migration and adhesion.[46] We also note that all experiments were conducted using MDA-MB-231 breast cancer cells, which were chosen for their phenotypic plasticity in response to their microenvironment.[33,37−40] Additionally, the assay requires that cells are in serum-free media to preserve the cRGD surface activity, as solutions containing as little as 1% FBS have been shown to reduce surface activity by 33-fold.[24]

Given that it is a significant problem in basic cancer research to understand what properties of the microenvironment elicit the Mesenchymal-to-Amoeboid Transition (MAT) and its role in cancer metastasis, these results highlight the importance of how both well-characterized surface activity and dynamic cellular metrics can reveal the subtle the differences in the spectrum of MDA-MB-231 phenotypes. As shown here, cancer cells can be directed to express a range of migratory phenotypes, thereby allowing drug dose−response curves to be generated for cells in both the highly migratory modes common to metastasis and the more stationary states more closely associated with slow growing tumors.

We also anticipate that cell-based therapeutics which rely on stem cells can now be explored systematically as a function of the engineered surface activity for reproducibly differentiating cells. We view this surface enhanced approach as a platform for maximizing the information gained from single-cell adhesion and migration assays before moving on to more complex (and more time-consuming) 2D and three-dimensional (3D) *in vivo* assays. The scanning stage live cell microscopy experimental approach coupled with completely automated self-supervised machine learning-based cell segmentation is well-suited for high throughput screening applications. The functionalization procedure has been successfully applied to 24-well plates and is adaptable to 96-well plates in the future.

CONCLUSIONS

The single-cell migration assay developed here combines chemically well-defined surfaces with morphological and migration analyses to both drive and interrogate cell phenotype. Application of this assay to MDA-MB-231 breast cancer cells led to the observation of distinct phenotypes in a label-free environment and without additional treatments in a reproducible manner. The quantitative control and reproducibility of this assay lends itself for use drug discovery and cell-based therapeutic design.

ASSOCIATED CONTENT

Data Availability Statement

The data that support these findings are available from the corresponding author upon reasonable request.

Supporting Information

The Supporting Information is available free of charge at https://pubs.acs.org/doi/10.1021/acs.langmuir.4c05135.

Fibronectin adsorption characterization, historical trend of surface activity graph; immunofluorescence staining of MDA-MB-231 cells on fibronectin-coated surfaces; distribution of focal adhesion measurements (PDF)

AUTHOR INFORMATION

Corresponding Author

Marc P. Raphael − *Naval Research Laboratory, Washington, District of Columbia 20375-5320, United States;* orcid.org/0000-0003-1794-5193; Email: marc.p.raphael.civ@us.navy.mil

Authors

Logan I. Kaler − *Naval Research Laboratory, Washington, District of Columbia 20375-5320, United States;* orcid.org/0000-0002-6502-5773

Michael C. Robitaille − *Naval Research Laboratory, Washington, District of Columbia 20375-5320, United States*

Joseph A. Christodoulides − *Naval Research Laboratory, Washington, District of Columbia 20375-5320, United States;* orcid.org/0000-0001-8828-4543

Patrick J. Calhoun − *Nanocrine, Inc., Frederick, Maryland 21704, United States*

Jeff M. Byers − *Naval Research Laboratory, Washington, District of Columbia 20375-5320, United States*

Complete contact information is available at: https://pubs.acs.org/10.1021/acs.langmuir.4c05135

Author Contributions

SPR studies: M.C.R., M.P.R. Chip functionalization: M.C.R., M.P.R., J.A.C. Cell culture: L.I.K, M.C.R. Live cell microscopy: M.C.R., M.P.R. Cell morphology and migration analysis: M.C.R., M.P.R., J.M.B. Immunofluorescence: L.I.K., M.C.R., P.J.C. Machine Vision Algorithm: M.C.R., M.P.R., J.M.B. Data Analysis: L.I.K., M.C.R., M.P.R., J.M.B. Article writing: L.I.K., M.C.R., M.P.R. All authors reviewed and edited the article.

Notes

The authors declare the following competing financial interest(s): Naval Research Laboratory co-authors (L.I.K., M.C.R., J.A.C., J.M.B., M.P.R.) participate in developing products for interfacing with and monitoring live cells via a Collaborative Research and Development Agreement (CRADA) between the US Government and Nanocrine, Inc (P.J.C) involving technology licensing and consultation.

ACKNOWLEDGMENTS

L.I.K. gratefully acknowledges support from the American Society for Engineering Education Postdoctoral Fellowship. M.C.R. gratefully acknowledges support from the Jerome and Isabella Karle Distinguished Scholar Fellowship Program. Funding for this project was provided by the Office of Naval Research through the Naval Research Laboratory's Basic Research Program.

REFERENCES

(1) Nevarez, A. J.; Hao, N. Quantitative Cell Imaging Approaches to Metastatic State Profiling. *Front. Cell Dev. Biol.* **2022**, *10*, No. 1048630.

(2) Daga, K. R.; Priyadarshani, P.; Larey, A. M.; Rui, K.; Mortensen, L. J.; Marklein, R. A. Shape up before You Ship out: Morphology as a Potential Critical Quality Attribute for Cellular Therapies. *Curr. Opin. Biomed. Eng.* **2021**, *20*, No. 100352.

(3) Dodkins, R.; Delaney, J. R.; Overton, T.; Scholle, F.; Frias-De-Diego, A.; Crisci, E.; Huq, N.; Jordan, I.; Kimata, J. T.; Findley, T.; Goldberg, I. G. A Rapid, High-Throughput, Viral Infectivity Assay Using Automated Brightfield Microscopy with Machine Learning. *SLAS Technol.* **2023**, *28* (5), 324−333.

(4) Grafton, F.; Ho, J.; Ranjbarvaziri, S.; Farshidfar, F.; Budan, A.; Steltzer, S.; Maddah, M.; Loewke, K. E.; Green, K.; Patel, S.; Hoey, T.; Mandegar, M. A. Deep Learning Detects Cardiotoxicity in a High-Content Screen with Induced Pluripotent Stem Cell-Derived Cardiomyocytes. *eLife* **2021**, *10*, No. e68714.
(5) Bray, M.-A.; Singh, S.; Han, H.; Davis, C. T.; Borgeson, B.; Hartland, C.; Kost-Alimova, M.; Gustafsdottir, S. M.; Gibson, C. C.; Carpenter, A. E. Cell Painting, a High-Content Image-Based Assay for Morphological Profiling Using Multiplexed Fluorescent Dyes. *Nat. Protoc.* **2016**, *11* (9), 1757−1774.
(6) Gordonov, S.; Hwang, M. K.; Wells, A.; Gertler, F. B.; Lauffenburger, D. A.; Bathe, M. Time Series Modeling of Live-Cell Shape Dynamics for Image-Based Phenotypic Profiling. *Integr. Biol.* **2016**, *8* (1), 73−90.
(7) Wang, W.; Douglas, D.; Zhang, J.; Kumari, S.; Enuameh, M. S.; Dai, Y.; Wallace, C. T.; Watkins, S. C.; Shu, W.; Xing, J. Live-Cell Imaging and Analysis Reveal Cell Phenotypic Transition Dynamics Inherently Missing in Snapshot Data. *Sci. Adv.* **2020**, *6* (36), No. eaba9319.
(8) Sasaki, H.; Takeuchi, I.; Okada, M.; Sawada, R.; Kanie, K.; Kiyota, Y.; Honda, H.; Kato, R. Label-Free Morphology-Based Prediction of Multiple Differentiation Potentials of Human Mesenchymal Stem Cells for Early Evaluation of Intact Cells. *PLoS One* **2014**, *9* (4), No. e93952.
(9) Pijuan, J.; Barceló, C.; Moreno, D. F.; Maiques, O.; Sisó, P.; Marti, R. M.; Macià, A.; Panosa, A. In Vitro Cell Migration, Invasion, and Adhesion Assays: From Cell Imaging to Data Analysis. *Front. Cell Dev. Biol.* **2019**, *7*, No. 107.
(10) Chen, Y.-C.; Allen, S. G.; Ingram, P. N.; Buckanovich, R.; Merajver, S. D.; Yoon, E. Single-Cell Migration Chip for Chemotaxis-Based Microfluidic Selection of Heterogeneous Cell Populations. *Sci. Rep.* **2015**, *5* (1), No. 9980.
(11) Kim, H. S.; Kumbar, S. G.; Nukavarapu, S. P. Biomaterial-Directed Cell Behavior for Tissue Engineering. *Curr. Opin. Biomed. Eng.* **2021**, *17*, No. 100260.
(12) Muncie, J. M.; Weaver, V. M.The Physical and Biochemical Properties of the Extracellular Matrix Regulate Cell Fate. In *Current Topics in Developmental Biology*; Elsevier, 2018; Vol. *130*, pp 1−37.
(13) Castilla-Casadiego, D. A.; Reyes-Ramos, A. M.; Domenech, M.; Almodovar, J. Effects of Physical, Chemical, and Biological Stimulus on h-MSC Expansion and Their Functional Characteristics. *Ann. Biomed. Eng.* **2020**, *48* (2), 519−535.
(14) Ferguson, L. P.; Diaz, E.; Reya, T. The Role of the Microenvironment and Immune System in Regulating Stem Cell Fate in Cancer. *Trends Cancer* **2021**, *7* (7), 624−634.
(15) DiMilla, P.; Stone, J.; Quinn, J.; Albelda, S.; Lauffenburger, D. Maximal Migration of Human Smooth Muscle Cells on Fibronectin and Type IV Collagen Occurs at an Intermediate Attachment Strength. *J. Cell Biol.* **1993**, *122* (3), 729−737.
(16) Palecek, S. P.; Loftus, J. C.; Ginsberg, M. H.; Lauffenburger, D. A.; Horwitz, A. F. Lntegrin-Ligand Binding Properties Govern Cell Migration Speed through Cellsubstratum Adhesiveness. *Nature* **1997**, *385* (6616), 537−540.
(17) Maheshwari, G.; Brown, G.; Lauffenburger, D. A.; Wells, A.; Griffith, L. G. Cell Adhesion and Motility Depend on Nanoscale RGD Clustering. *J. Cell Sci.* **2000**, *113* (10), 1677−1686.
(18) Rajagopalan, P.; Marganski, W. A.; Brown, X. Q.; Wong, J. Y. Direct Comparison of the Spread Area, Contractility, and Migration of Balb/c 3T3 Fibroblasts Adhered to Fibronectin- and RGD-Modified Substrata. *Biophys. J.* **2004**, *87* (4), 2818−2827.
(19) Shabbir, S. H.; Eisenberg, J. L.; Mrksich, M. An Inhibitor of a Cell Adhesion Receptor Stimulates Cell Migration. *Angew. Chem., Int. Ed.* **2010**, *49* (42), 7706−7709.
(20) Charras, G.; Sahai, E. Physical Influences of the Extracellular Environment on Cell Migration. *Nat. Rev. Mol. Cell Biol.* **2014**, *15* (12), 813−824.
(21) Missirlis, D.; Haraszti, T.; Scheele, C. V. C.; Wiegand, T.; Diaz, C.; Neubauer, S.; Rechenmacher, F.; Kessler, H.; Spatz, J. P. Substrate Engagement of Integrins A5β1 and Avβ3 Is Necessary, but Not Sufficient, for High Directional Persistence in Migration on Fibronectin. *Sci. Rep.* **2016**, *6* (1), No. 23258.
(22) Schvartzman, M.; Palma, M.; Sable, J.; Abramson, J.; Hu, X.; Sheetz, M. P.; Wind, S. J. Nanolithographic Control of the Spatial Organization of Cellular Adhesion Receptors at the Single-Molecule Level. *Nano Lett.* **2011**, *11* (3), 1306−1312.
(23) Attwood, S. J.; Cortes, E.; Haining, A. W. M.; Robinson, B.; Li, D.; Gautrot, J.; Del Río Hernández, A. Adhesive Ligand Tether Length Affects the Size and Length of Focal Adhesions and Influences Cell Spreading and Attachment. *Sci. Rep.* **2016**, *6* (1), No. 34334.
(24) Robitaille, M. C.; Christodoulides, J. A.; Liu, J.; Kang, W.; Byers, J. M.; Raphael, M. P. Problem of Diminished cRGD Surface Activity and What Can Be Done about It. *ACS Appl. Mater. Interfaces* **2020**, *12* (17), 19337−19344.
(25) Peter, B.; Farkas, E.; Forgacs, E.; Saftics, A.; Kovacs, B.; Kurunczi, S.; Szekacs, I.; Csampai, A.; Bosze, S.; Horvath, R. Green Tea Polyphenol Tailors Cell Adhesivity of RGD Displaying Surfaces: Multicomponent Models Monitored Optically. *Sci. Rep.* **2017**, *7* (1), No. 42220.
(26) Kovács, K. D.; Szittner, Z.; Magyaródi, B.; Péter, B.; Szabó, B.; Vörös, A.; Kanyó, N.; Székács, I.; Horvath, R. Optical Sensor Reveals the Hidden Influence of Cell Dissociation on Adhesion Measurements. *Sci. Rep.* **2024**, *14* (1), No. 11719.
(27) Di Cio, S.; Gautrot, J. E. Cell Sensing of Physical Properties at the Nanoscale: Mechanisms and Control of Cell Adhesion and Phenotype. *Acta Biomater.* **2016**, *30*, 26−48.
(28) Mrksich, M. A Surface Chemistry Approach to Studying Cell Adhesion. *Chem. Soc. Rev.* **2000**, *29* (4), 267−273.
(29) Robitaille, M. C.; Christodoulides, J. A.; Calhoun, P. J.; Byers, J. M.; Raphael, M. P. Interfacing Live Cells with Surfaces: A Concurrent Control Technique for Quantifying Surface Ligand Activity. *ACS Appl. Bio Mater.* **2021**, *4* (11), 7856−7864.
(30) Robitaille, M. C.; Byers, J. M.; Christodoulides, J. A.; Raphael, M. P. Self-Supervised Machine Learning for Live Cell Imagery Segmentation. *Commun. Biol.* **2022**, *5* (1), No. 1162.
(31) Wu, P.-H.; Giri, A.; Wirtz, D. Statistical Analysis of Cell Migration in 3D Using the Anisotropic Persistent Random Walk Model. *Nat. Protoc.* **2015**, *10* (3), 517−527.
(32) Stirling, D. R.; Swain-Bowden, M. J.; Lucas, A. M.; Carpenter, A. E.; Cimini, B. A.; Goodman, A. CellProfiler 4: Improvements in Speed, Utility and Usability. *BMC Bioinf.* **2021**, *22* (1), No. 433.
(33) Rodríguez-Cruz, D.; Boquet-Pujadas, A.; López-Muñoz, E.; Rincón-Heredia, R.; Paredes-Díaz, R.; Flores-Fortis, M.; Olivo-Marin, J.-C.; Guillén, N.; Aguilar-Rojas, A. Three-Dimensional Cell Culture Conditions Promoted the Mesenchymal-Amoeboid Transition in the Triple-Negative Breast Cancer Cell Line MDA-MB-231. *Front. Cell Dev. Biol.* **2024**, *12*, No. 1435708.
(34) Ikenouchi, J.; Aoki, K. A Clockwork Bleb: Cytoskeleton, Calcium, and Cytoplasmic Fluidity. *FEBS J.* **2022**, *289* (24), 7907−7917.
(35) Graziani, V.; Rodriguez-Hernandez, I.; Maiques, O.; Sanz-Moreno, V. The Amoeboid State as Part of the Epithelial-to-Mesenchymal Transition Programme. *Trends Cell Biol.* **2022**, *32* (3), 228−242.
(36) Yamada, K. M.; Sixt, M. Mechanisms of 3D Cell Migration. *Nat. Rev. Mol. Cell Biol.* **2019**, *20* (12), 738−752.
(37) Bemmerlein, L.; Deniz, I. A.; Karbanová, J.; Jacobi, A.; Drukewitz, S.; Link, T.; Göbel, A.; Sevenich, L.; Taubenberger, A. V.; Wimberger, P.; Kuhlmann, J. D.; Corbeil, D. Decoding Single Cell Morphology in Osteotropic Breast Cancer Cells for Dissecting Their Migratory, Molecular and Biophysical Heterogeneity. *Cancers* **2022**, *14* (3), No. 603.
(38) Huang, Y. L.; Tung, C.; Zheng, A.; Kim, B. J.; Wu, M. Interstitial Flows Promote Amoeboid over Mesenchymal Motility of Breast Cancer Cells Revealed by a Three Dimensional Microfluidic Model. *Integr. Biol.* **2015**, *7* (11), 1402−1411.
(39) Geum, D. T.; Kim, B. J.; Chang, A. E.; Hall, M. S.; Wu, M. Epidermal Growth Factor Promotes a Mesenchymal over an

https://doi.org/10.1021/acs.langmuir.4c05135
Langmuir 2025, 41, 13763−13773

Amoeboid Motility of MDA-MB-231 Cells Embedded within a 3D Collagen Matrix. *Eur. Phys. J. Plus* **2016**, *131* (1), No. 8.
(40) Wang, L.; Xu, C.; Liu, X.; Yang, Y.; Cao, L.; Xiang, G.; Liu, F.; Wang, S.; Liu, J.; Meng, Q.; Jiao, J.; Niu, Y. TGF-B1 Stimulates Epithelial−Mesenchymal Transition and Cancer-Associated Myoepithelial Cell during the Progression from in Situ to Invasive Breast Cancer. *Cancer Cell Int.* **2019**, *19* (1), No. 343.
(41) Ecker, N.; Kruse, K. Excitable Actin Dynamics and Amoeboid Cell Migration. *PLoS One* **2021**, *16* (2), No. e0246311.
(42) Maheshwari, G.; Wells, A.; Griffith, L. G.; Lauffenburger, D. A. Biophysical Integration of Effects of Epidermal Growth Factor and Fibronectin on Fibroblast Migration. *Biophys. J.* **1999**, *76* (5), 2814−2823.
(43) Liu, Z.; Lee, S. J.; Park, S.; Konstantopoulos, K.; Glunde, K.; Chen, Y.; Barman, I. Cancer Cells Display Increased Migration and Deformability in Pace with Metastatic Progression. *FASEB J.* **2020**, *34* (7), 9307−9315.
(44) He, J.; Shen, R.; Liu, Q.; Zheng, S.; Wang, X.; Gao, J.; Wang, Q.; Huang, J.; Ding, J. RGD Nanoarrays with Nanospacing Gradient Selectively Induce Orientation and Directed Migration of Endothelial and Smooth Muscle Cells. *ACS Appl. Mater. Interfaces* **2022**, *14* (33), 37436−37446.
(45) Song, Z.; Lin, Y.; Zhang, X.; Feng, C.; Lu, Y.; Gao, Y.; Dong, C. Cyclic RGD Peptide-Modified Liposomal Drug Delivery System for Targeted Oral Apatinib Administration: Enhanced Cellular Uptake and Improved Therapeutic Effects. *Int. J. Nanomed.* **2017**, *12*, 1941−1958.
(46) Beres, B.; Kovacs, K. D.; Kanyo, N.; Peter, B.; Szekacs, I.; Horvath, R. Label-Free Single-Cell Cancer Classification from the Spatial Distribution of Adhesion Contact Kinetics. *ACS Sens.* **2024**, *9* (11), 5815−5827.

https://doi.org/10.1021/acs.langmuir.4c05135
Langmuir 2025, 41, 13763−13773